

See discussions, stats, and author profiles for this publication at: <https://www.researchgate.net/publication/307977313>

Prediction of Changes in Urban Micro-Climate using Remote Sensing Data and Artificial Neural Network Model

Article in *Wulfenia* · December 2015

CITATION

1

READS

118

3 authors, including:



Sundarakumar Kusuma

Usha Rama College of Engineering & Technology, Andhra Pradesh, India

31 PUBLICATIONS 82 CITATIONS

SEE PROFILE

Some of the authors of this publication are also working on these related projects:



Modeling of Urban Climate of new capital city of Andhra Pradesh [View project](#)

Prediction of Changes in Urban Micro-Climate using Remote Sensing Data and Artificial Neural Network

Model

***Kusuma. Sundara Kumar**¹, **Pinnamaneni. Udaya Bhaskar**², **Kollipara. Padma Kumari**³

¹Research Scholar, Department of Civil Engineering, JNT University-Kakinada, Andhra Pradesh, India, 533003

^{2 & 3} Professor, Department of Civil Engineering, JNT University-Kakinada, Andhra Pradesh, India, 533003

*Corresponding Author: Tel: +91 9440112013, E-mail: skkusuma123@gmail.com

Abstract

Changes in urban microclimate can have adverse effects on the city dwellers in many ways including thermal discomfort and loss of life due to heat waves, development of air pollutants, etc. Microclimate of urban area primarily depends on the land use and land cover (LULC). Conversion of greenery cover into impervious built up surfaces increase the heat retaining capacity and result in increased land surface temperature (LST) which in turn increase the local air temperature. This paper presents a new approach to the application of artificial neural network (ANN) for prediction of LST image from LULC image. Landsat TM images of the study area for 2001 and 2010 are used to develop LULC and LST images. A feed forward back propagation ANN model with Levenberg-Marquardt training algorithm has been developed to simulate and predict the LST image from LULC image data. Along with LULC, elevation, latitude and longitude data are also given as inputs to optimize the model. The data sets of 2001 are used for training and that of 2010 for testing the model. The model efficiency was found to be of 81.621%. LST image of the year 2015 was predicted from LULC image using the model.

Keywords: Urban microclimate, Land surface temperature, Urban heat island, Land use/land cover, Artificial neural network, Landsat data.

1 INTRODUCTION

Rapid urbanization and unplanned development of cities have led to several urban environmental issues. Development an intense urban heat island (UHI) is one of the significant problems. Prediction of spatial variation of LST plays a key role in the

urban thermal environmental management and particularly useful for mitigation of urban heat island (UHI) effect. The urban air temperature is gradually rising in all cities in the world because of the drastic reduction in the greenery in cities. The change of land use from agriculture to industry, green area to built-up structures and artificial surfaces covered by asphalt and concrete, have brought changes in the natural surface of the earth which affect local environmental conditions.¹ Modification of land-cover in urban areas with built-up surfaces can cause the local air and surface temperatures to raise several degrees higher than the simultaneous temperatures of the surrounding rural areas or villages.²⁻⁴ This is due to heat retaining and radiating capabilities of the artificial materials used to cover the land surface. This effect is often referred to as the urban heat island and has been documented for over 150 years.⁵ The phenomenon of the urban heat island is one of the most well known forms of anthropogenic climate modification, which is increasingly observed in cities due to growth of population and urban sprawl.⁶ The higher temperatures in urban heat islands increase air conditioning demands, raise air pollution levels, modify precipitation patterns⁷⁻⁹ and also serve as a trap for atmospheric pollutants, which contribute to smog, deteriorate the quality of life and has a socio-economic impact in the urbanized areas.¹⁰ As a result, the magnitude and pattern of UHI effects have been major concerns of many urban climatologic studies. Consequently, the prediction of the urban heat island behaviour has gained a significant attention.¹¹ Although a number of modeling approaches for the urban heat island do exist the complexity of the phenomenon, and the increased cost and computational time of the analytical modeling approaches have led to the exploration of other prediction methods.¹²

The surface temperature is of prime importance to the study of urban climate, not only in obtaining boundary conditions of the atmosphere, but also in understanding the environmental conditions necessary for human beings.¹³ LST modulates the air temperature of the lower layer of urban atmosphere, and is a primary factor in determining surface radiation and energy exchange, the internal climate of buildings, and human comfort levels in the cities¹⁴. Understanding the distribution of Land Surface Temperature and its spatial variation will be helpful to decipher its mechanism and find out possible solution. LST is an important parameter in the studies of urban thermal environment and dynamics. The LST of urban surfaces is closely related to the distribution of LULC characteristics.¹⁵⁻¹⁷

The relationship between LST and vegetation indices, such as Normalized Difference Vegetation Index (NDVI), has been extensively documented in the literature.¹⁸⁻²¹ The NDVI-temperature relationship has also been utilized in various studies to derive or evaluate fractional vegetation cover and surface soil water content for climate modeling.²²⁻²⁴ Many studies reveal that there is always a negative relationship between LST and vegetation indices.²⁵⁻²⁹

LST of an area can be estimated by processing thermal band data of satellite imagery. Satellite-measured LST has been utilized in various heat-balance, climate modeling, and global-change studies because it is determined by the effective

radiating temperature of the Earth's surface, which controls surface heat and water exchange with the atmosphere. Remotely sensed thermal infrared (TIR) data are a unique source of information to define the occurrence of surface heat islands, which are related to canopy layer heat islands. The 120 m resolution Landsat TM (and later ETM+ data of 60 m) TIR data have also been extensively utilized to derive LSTs and to study UHIs.³⁰⁻³¹ The thermal differences between urban and rural areas appear even in the case of relatively small towns.³² Traditionally, UHI analysis uses air temperature data observed at a standard height (1.5–2 m above the ground), while satellite images provide thermal information at ground-level. Based on observed air temperature data, the maximum UHI intensity occurs a few hours after sunset, while the most intense UHI can be detected during day-time when remotely sensed data are used.³³⁻³⁴

Artificial neural networks (ANNs), which are increasingly receiving attention in solving complex practical problems, are known as universal function approximators.³⁵⁻³⁶ They are capable of approximating any continuous nonlinear functions to some arbitrary accuracy.³⁷ Its applications are numerous in various fields including engineering, management, health, biology and even social sciences.³⁸⁻⁴⁴ Artificial neural networks have been applied in many different environmental sectors, especially in forecasting meteorological parameters.⁴⁵

Urban climate and environmental studies will be impossible, without TIR sensors of global imaging capacity. At the present, there are few sensors that have such thermal IR capabilities. The TM sensor onboard Landsat 5 has been acquiring images of the Earth nearly continuously from March 1984 to January 2013, with a TIR band of 120 m resolution, and is well past the mission's life expectancy. Another TIR sensor that has global imaging capacity is with Landsat 7 ETM+. On May 31, 2003, the ETM+ Scan Line Corrector (SLC) failed permanently. Although it is still capable of acquiring useful image data, with the SLC turned off, a lot of information was lost due to black stripes. Development of LST images from such imagery becomes less accurate. NASA has teamed up with United States Geological Services (USGS) to focus on the Landsat Data Continuity Mission (LDCM), which is resulted in launching Landsat-8 in 2013. Hence from 2003 to 2013, Landsat imagery which has a thermal band becomes less useful. Other data obtained from ASTER, MODIS will have very low resolution not suitable for study at a local level.

Towards a solution to this kind of problem of scarcity of TIR data, an attempt was made to predict LST image from LULC image. This paper deals with the development an artificial neural network model for prediction of LST image from LULC image. The advantage of the model is that model requires only LULC image to get LST image. LULC image can be obtained from multispectral data. The following sections briefly outlined the methodology to develop LULC, NDVI and LST images from raw Landsat imagery. The development of ANN model was also presented, and the results obtained were discussed.

2 STUDY AREA AND DATA

For the present work, Vijayawada, the capital city of Andhra Pradesh state in India is taken as the case study. The city is located on the bank of Krishna River with latitude 16⁰31'1'' N and longitude 80⁰ 39'1'' E. It is a historical city. It is known as the business capital of the state. The city is rapidly expanding with real estate boom in the recent past. The city is well known for recording high temperatures in summer. Vijayawada city is experiencing remarkable UHI and the difference between the temperatures of urban core and the rural village is about 10⁰C. UHI is one of the upcoming urban climate-related problems developing in the city. An understanding of the intensity and extent of UHI is useful for proposing the mitigation measures. For the present study, Landsat images were procured from Earth explorer of USGS website. The visible and thermal bands with high resolution are the important qualities of the Landsat imagery which were the reason for selection of imagery. The details of the imagery collected are given in Table 1.

Table 1 Details of Imagery procured from USGS

| Sl. No | Date | Satellite/Sensor | No of Bands | Reference system / Path/Row | Resolution | |
|--------|-------------|--------------------|-------------|-----------------------------|------------|---------|
| | | | | | multi | thermal |
| 1 | 31-10- 2001 | Landsat7/ETM+ | 8 | WRS-II/142/49 | 30m | 60m |
| 2 | 26-06-2010 | Landsat7/ETM+ | 8 | WRS-II/142/49 | 30m | 60m |
| 3 | 23-05-2015 | Landsat8/OLI- TIRS | 11 | WRS-II/142/49 | 30m | 100m |

3 METHODOLOGY

The objective of the present study is to develop an ANN based model to retrieve LST image from LULC image. After down loading from the web sources, the Landsat image data is first pre-processed and enhanced for attaining better image quality. The study area has been extracted from the image. Using this clipped image, LULC, NDVI and LST images are developed. For all these operations, ERDAS Imagine or similar image-processing software can be used. Now the image data is converted into digital data (discrete numerical) using Arc GIS. Next step is the coding of ANN model in MATLAB for inputting the LULC, NDVI and Lat/ Long data to the model and getting LST as output. Different sets of data are used for training and testing the model. The data of 2001 is used for training and data of 2010 is used for testing. The LST images developed using ERDAS are compared with the LST images obtained from the ANN model to assess the model performance. Regression analysis is performed on the image data of observed (developed by ERDAS) and predicted

(given by ANN model) for both training and testing phases. Detailed procedures are given in the following sections.

3.1 Development of LULC and NDVI images

The Landsat images downloaded for the years 2001, and 2010 consists of 8 bands, which include visible and thermal infrared bands. These images are ideal for developing LULC images as well as LST images. Cloud free images selected from the archives are used. The image data available in the form of a number of bands are first stacked, pre-processed and are performed certain image enhancement techniques like histogram equalization to improve the quality of the image. Both the images are brought to the same pixel resolution by using resampling technique. The obtained image is used to extract the study area using rectangular shaped ‘area of interest’ in which the Vijayawada city, and its suburban areas are included. The Landsat images of the above-mentioned dates are used to develop land use/cover maps of the study area. Five land use/cover classes are identified viz., built-up, dense vegetation, light vegetation, bare soil/sand and water. Initially, unsupervised classification technique was used to classify the image to have a better understanding about the different groups of pixels present in the image. Finally supervised classification technique was used to classify the image. Field data collected with hand held GPS, Google Earth images and Survey of India topo-sheets are used for reference. The intensity and richness of vegetation cover on the land surface is better interpreted by NDVI image. It is developed by the band ratio given in equation 1.

$$NDVI = \frac{(BAND\ 4 - BAND\ 3)}{(BAND\ 4 + BAND\ 3)} \quad (1)$$

3.2 Development of LST images

The majority of urban study researchers are interested in relative LST measurements, i.e., in mapping the spatial variations of LST and identification of hotspots in the urban heat island. Landsat satellite’s thermal infrared sensors measure ‘top of the atmosphere’ radiances, from which brightness temperatures (also known as blackbody temperatures) can be derived using Plank's law.⁴⁶ A widely used method result from the Landsat-7 Science Data User's Handbook, developed by the Landsat Project Science Office at NASA's Goddard Space Flight Centre.⁴⁷ After converting the digital numbers (DN) of the Landsat ETM+ Band 6 into absolute radiance values, at-satellite brightness temperatures (i.e., blackbody temperature) are computed under the assumption of unity emissivity and using pre-launch calibration constants, which is followed by a correction for spectral emissivity according to the nature of land cover/use.

The digital number (DN) of thermal infrared band is converted into spectral radiance ($L\lambda$) using the equation 2 supplied by the Landsat user's hand book.

$$L\lambda = \left\{ \frac{LMAX - LMIN}{QCALMAX - QCALMIN} \right\} * DN - 1 + LMIN \quad (2)$$

LMAX = the spectral radiance scaled to QCALMAX in $W / (m^2 * sr * \mu m)$

LMIN = the spectral radiance scaled to QCALMIN in $W / (m^2 * sr * \mu m)$

QCALMAX = the maximum quantized calibrated pixel value (corresponding to LMAX) in DN = 255

QCALMIN = the minimum quantized calibrated pixel value (corresponding to LMIN) in DN = 1

LMAX and LMIN are obtained from the Meta data file available with the image are 15.303 and 1.2378 respectively for Landsat5 /TM and 12.65, 3.2 for Landsat7 /ETM+. The effective at-sensor brightness temperature (TB) also known as black body temperature is obtained from the spectral radiance using Plank's inverse function given in equation 3.

$$TB = \frac{K2}{\ln\left(1 + \frac{K1}{L\lambda}\right)} \quad (3)$$

The calibration constants K1 and K2 obtained from Landsat data user's manual are 607.76 and 1260.56 for Landsat5 /TM and 666.09, 1282.71 for Landsat7/ETM+.

Emissivity is the inherent characteristic of the material which identifies its thermal behaviour. For ground objects from passive sensor data emissivity data, can be estimated using different techniques. Among those techniques are normalized emissivity method⁴⁸, thermal spectral indices⁴⁹, spectral ratio method⁵⁰, Alpha residual method⁵¹, NDVI method⁵², classification-based estimation, and the temperature-emissivity separation method.⁵³⁻⁵⁴

In this work an Emissivity image is developed using the NDVI image by assigning emissivity values for different types of land cover. First NDVI image has been classified into five classes corresponding to the five LULC classes, using unsupervised classification technique. Using this NDVI classified image, an emissivity image has been developed. For this a conditional logic was applied in the ERDAS model maker to assign emissivity values based on the NDVI class. The emissivity values assigned to these five classes are 0.92 for built-up land, 0.95 for bare soil, and 0.96 for light vegetation, 0.99 for thick vegetation and 0.98 for water. The resulting emissivity image based on NDVI classes is used to develop final land surface temperature image using equation 4.

$$LST = \frac{TB}{1 + (\lambda * TB / \rho) * \ln \epsilon} \quad (\text{Unit: Kelvin}) \quad (4)$$

Where, λ is the wavelength of the emitted radiance which is equal to $11.5 \mu m$. $\rho = h.c/\sigma$, σ = Stefan Boltzmann's constant which is equal to $5.67 \times 10^{-8} Wm^{-2} K^{-4}$, h = Plank's constant ($6.626 \times 10^{-34} J Sec$), c = velocity of light ($2.998 \times 10^8 m/sec$) and ϵ

is spectral emissivity. For all the calculations at pixel level of the image, models are developed using Spatial Modeller module of ERDAS Imagine.

3.3 Development of ANN model

LULC image can be developed from almost any kind of satellite data which obviously will have information in visible band, but it is not possible to derive LST image without thermal infrared band data. Hence the main objective here is to develop LST image from LULC image without using thermal band imagery. This kind of work will greatly help in producing LST images without using the thermal band data. If future LULC got predicted for any area, this model will give the LST image of the same area which would help in thermal environmental studies of the present and the future.

For this a feed forward back propagation ANN model with Levenberg-Marquardt training algorithm has been developed by writing code in MATLAB to simulate and predict the LST image from LULC image. Surface temperature value depends on the type of land surface and hence the model is trained with LULC and LST values to develop Weightages and bias which can be used later for predicting LST. In this model additional data like elevation, latitude and longitude are also included in the input layer to improve model's efficiency. First the LULC and LST images obtained from processing the Landsat images of dates 31-10-2001 and 26-06-2010 are re-sampled to the same pixel size so that all images used in the model will have equal number of pixels. The size of the image clipped for the study area is 590 columns and 430 rows. Elevation image was down loaded from Shuttle Radar Topography Mission (SRTM) of USGS website; this image contains elevation values in metres.

Using the pixel values, each image data has been converted into discrete digital data that is ASCII in Arc GIS for use in the model. Now these matrices containing 590 X 430 numbers are converted in to single strings of 253,700 values each in the MATLAB. Hence for each image 253,700 pixel values are given as input string. The LULC image will have 1 to 6 values corresponding to the 6 classes; elevation image will have 253,700 pixels whose values are in meters. Similarly LST image will contain the same number of pixel values of temperature in degrees Kelvin ranging from low (299 K) to high (320 K). Latitude and Longitude values are converted from degree-minute-second format to decimal value for feeding the model as input. The model efficiency is verified for different input combinations given in the Table 2. When all the four input parameters viz., LULC, elevation, Latitude and Longitude are given as inputs to the model, it is found to give maximum efficiency and hence selected as the best one. The model architecture showing arrangement of the input, output and hidden layers is shown in Fig. 1.

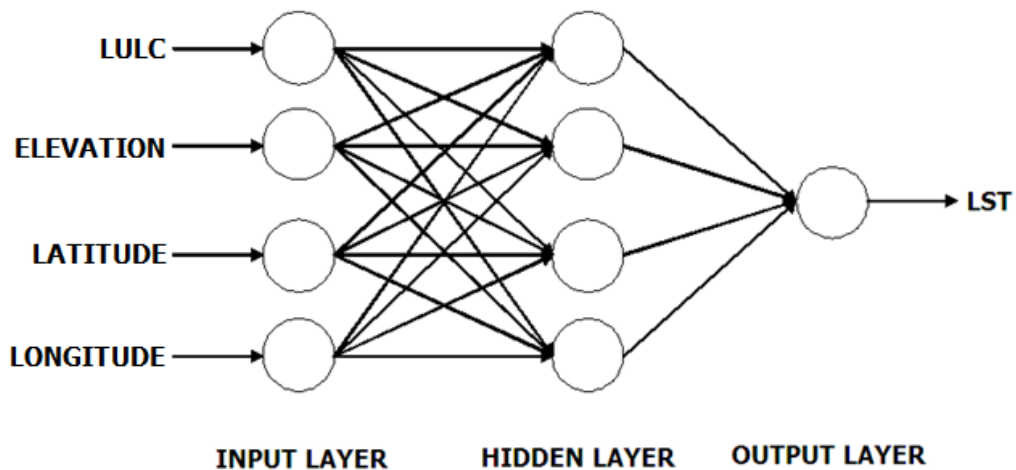


Fig. 1 ANN model architecture

For training the model LULC and LST images data of 2001 are used. For testing the model LULC and LST images data of 2010 are used. The values of latitude and longitude of pixels were obtained by using a model in Arc GIS. The output of the ANN model obtained from MATLAB, which is in the form of discrete data, is converted back into image format using Arc GIS. The generalized flow charts showing the training and testing of the ANN model is shown in the following Fig.2 & Fig.3.

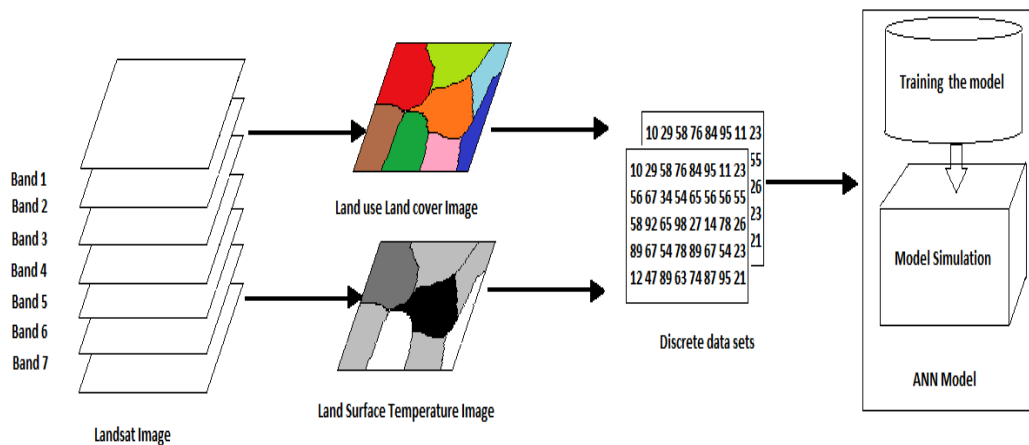


Fig. 2 Flow chart showing the training of the ANN model

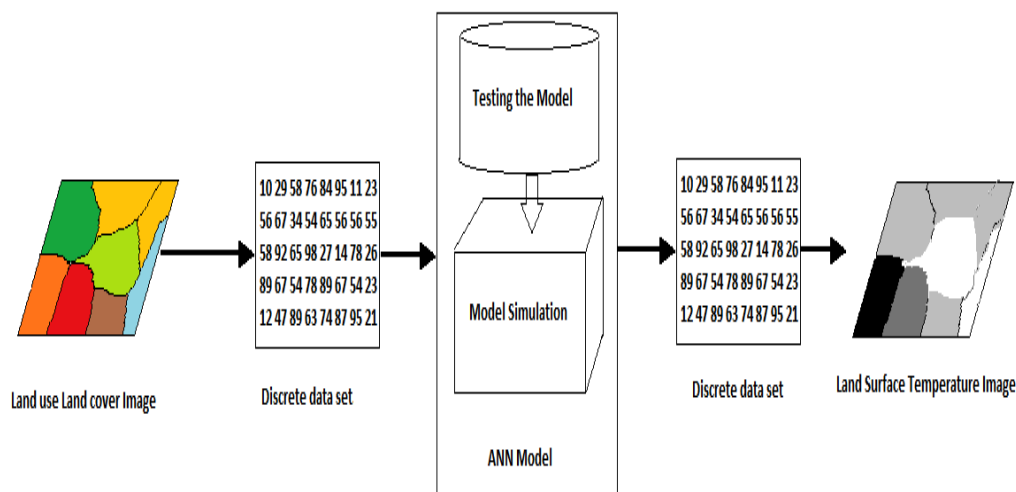


Fig. 3 Flow chart showing the testing of the ANN model

4 RESULTS AND DISCUSSION

All the final products of images developed are presented in this section, and results were discussed critically. The LULC images developed from the “supervised classification” method adopted, and the NDVI images obtained from ERDAS Imagine are presented below. The actual LST image developed from the thermal band of Landsat satellite image using ERDAS Imagine are presented here. The Predicted LST images obtained from the trained ANN model were also presented here. The actual and predicted images were compared, and correlation studies were carried out to establish the validity. The LST image obtained from ANN model without using the thermal band in ERDAS Imagine is also provided for the year 2015.

4.1 LULC, NDVI, LST Images

Classified images showing the five LULC classes in the study area for the year 2001 and corresponding NDVI images are shown in Fig. 4(a) and 4(b). Similarly classified images in the year 2010 and its NDVI images are shown in Fig. 5(a) and 5(b). The classified images were compared with the actual data comprising Government published data and Google Earth, to check the accuracy. The overall classification accuracy achieved in the supervised classification process is 80% and Kappa statistic obtained is 0.729. NDVI values vary from -0.98 to 0.983 for the year 2001 and from -0.985 to 0.992 for the year 2010.

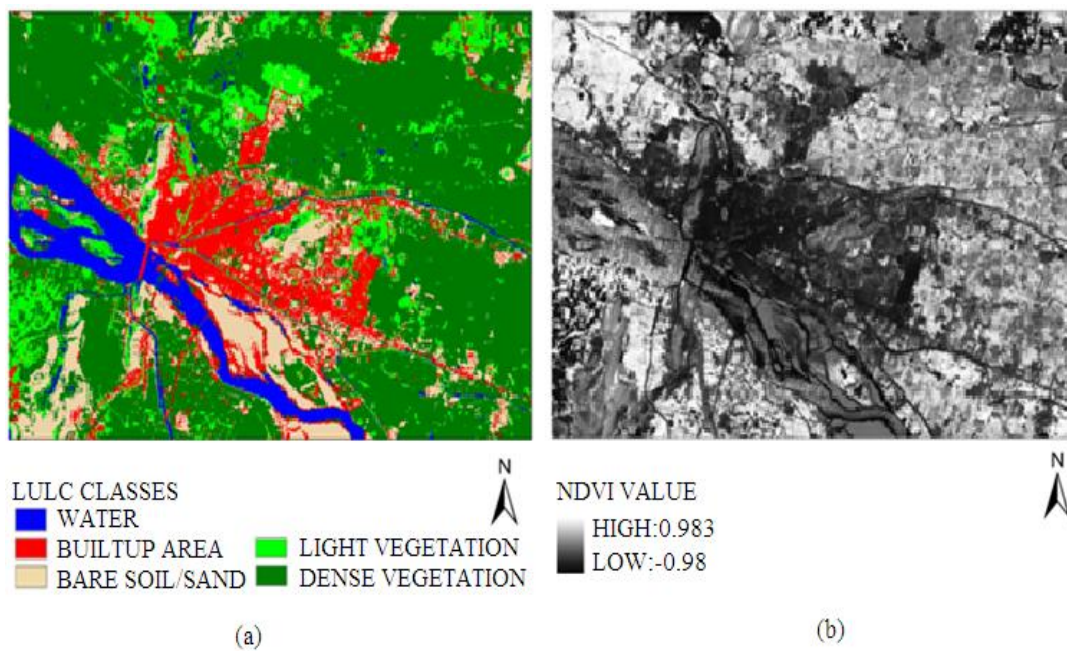


Fig. 4 (a) LULC image of 2001 (b) NDVI image of 2001

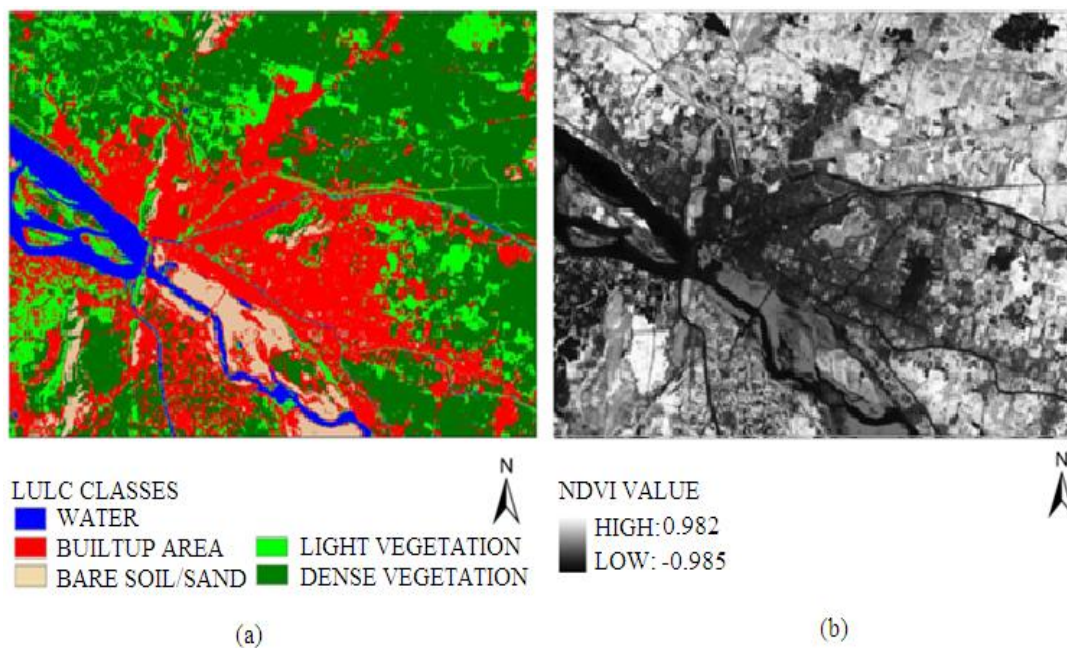


Fig.5 (a) LULC image of 2010 (b) NDVI image of 2010

4.2 Model Performance

Three models are developed with different sets of input parameters and trained and tested with 2001 and 2010 data respectively. Model no.1 consists of LULC as input and LST as output. LULC class values and elevation values are given as input in Model no.2 with LST as output. Model no.3 takes LULC, elevation, latitude and longitude as inputs and produces LST as output. As the surface temperature is greatly influenced by the location of the area, addition of latitude and longitude will definitely have a positive impact on the performance of the model.

The performances of the models are evaluated by studying the observed and predicted values using the statistical parameters viz., Coefficient of determination (R^2), root mean square error (RMSE), mean absolute error (MAE) and Model Efficiency (E_{NS}). The details of models and input parameter combinations are presented in Table 2. The Goodness-of-fit statistics for the observed and predicted LST for training with 2001 data are presented in Table 3 and the Goodness-of-fit statistics for the observed and predicted LST for testing with 2010 data are presented in Table 4. The feed forward back propagation ANN model with the Levenberg-Marquardt training algorithm is run with 2001 data for training and 2010 data for testing. The model produced maximum efficiency when the hidden nodes are limited to 4; corresponding RMSE is the least one. Hence the model with four input parameters viz., LULC, elevation, latitude, longitude and four hidden nodes was selected as the best one. The variation of model efficiency and RMSE with a number of hidden nodes is shown in Fig.6.

Table 2 Details of Models and Input Parameters

| Model No | Input Combinations | Output |
|----------|----------------------------|--------|
| 1 | LULC | LST |
| 2 | LULC, ELEVATION | LST |
| 3 | LULC, ELEVATION, LAT, LONG | LST |

Table 3 Goodness-of-fit statistics for the actual and predicted LST for training with 2001 data

| Model No | MAE | E_{NS} | RMSE | R^2 |
|----------|--------|----------|--------|-------|
| 1 | 11.078 | 0.713 | 13.434 | 0.718 |
| 2 | 8.782 | 0.808 | 10.982 | 0.809 |
| 3 | 8.552 | 0.816 | 10.756 | 0.821 |

Table 4. Goodness-of-fit statistics for the actual and predicted LST for testing with 2010 data

| Model No | MAE | E_{NS} | RMSE | R^2 |
|----------|--------|----------|--------|-------|
| 1 | 11.243 | 0.693 | 14.238 | 0.800 |
| 2 | 9.283 | 0.721 | 13.046 | 0.807 |
| 3 | 9.489 | 0.779 | 11.595 | 0.825 |

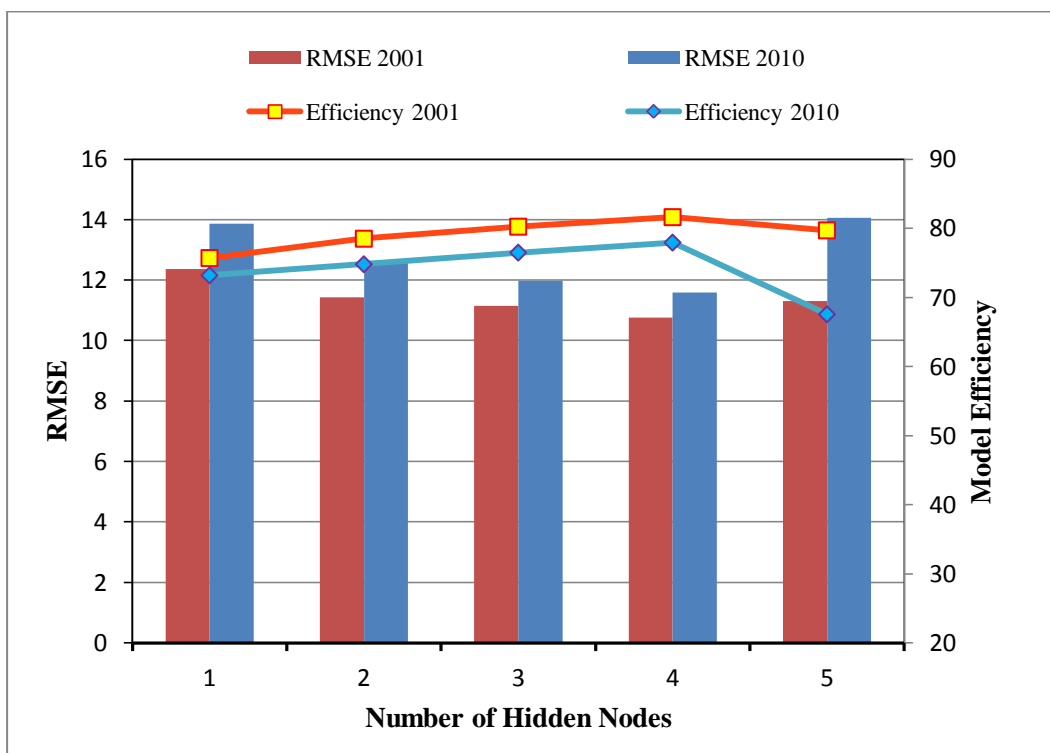


Fig. 6 Variation of model efficiency and RMSE with number of hidden nodes

4.3 Output LST Images

The actual LST images developed by Landsat data using ERDAS imagine for the year 2001 and 2010, and the corresponding predicted LST images obtained from the ANN model are presented in Figures 7(a) to 7(d). The minimum and maximum values of LST range from 299 to 320 K. The predicted image of LST is very similar to the actual LST image. To validate the model efficiency, statistical analysis was performed on sample data sets taken from certain random columns and rows in the image. The corresponding pixel values of the actual and predicted LST images were taken, and regression analysis was done and scatter plots are developed for actual observed and predicted LST values. The scatter plots are shown in Fig. 8 (a) to 8(d). The R^2 values obtained from scatter plots for the 2001 are 0.8352 and 0.8116 and for 2010 are 0.8361 and 0.7686. From these values it is understood that the model is predicting well.

4.4 Prediction of LST image of 2015

After ascertaining the satisfactory performance of the developed ANN model, LULC image of the year 2015 was given as input to predict the LST image of the year 2015. The LULC image for the year 2015 and the predicted LST images for the year 2015 are shown in Fig. 9 (a) and (b). Like this, LST images of the future dates can also be predicted by this model provided the LULC image of the future date.

The predicted LST image can give valuable information for the mitigation efforts to be made to counteract the urban heat island effect. It can mainly show the areas and their locations of elevated temperature where necessary action is to be initiated with high priority. Hence this kind of prediction of LST image is very useful for urban planners for environmental management.

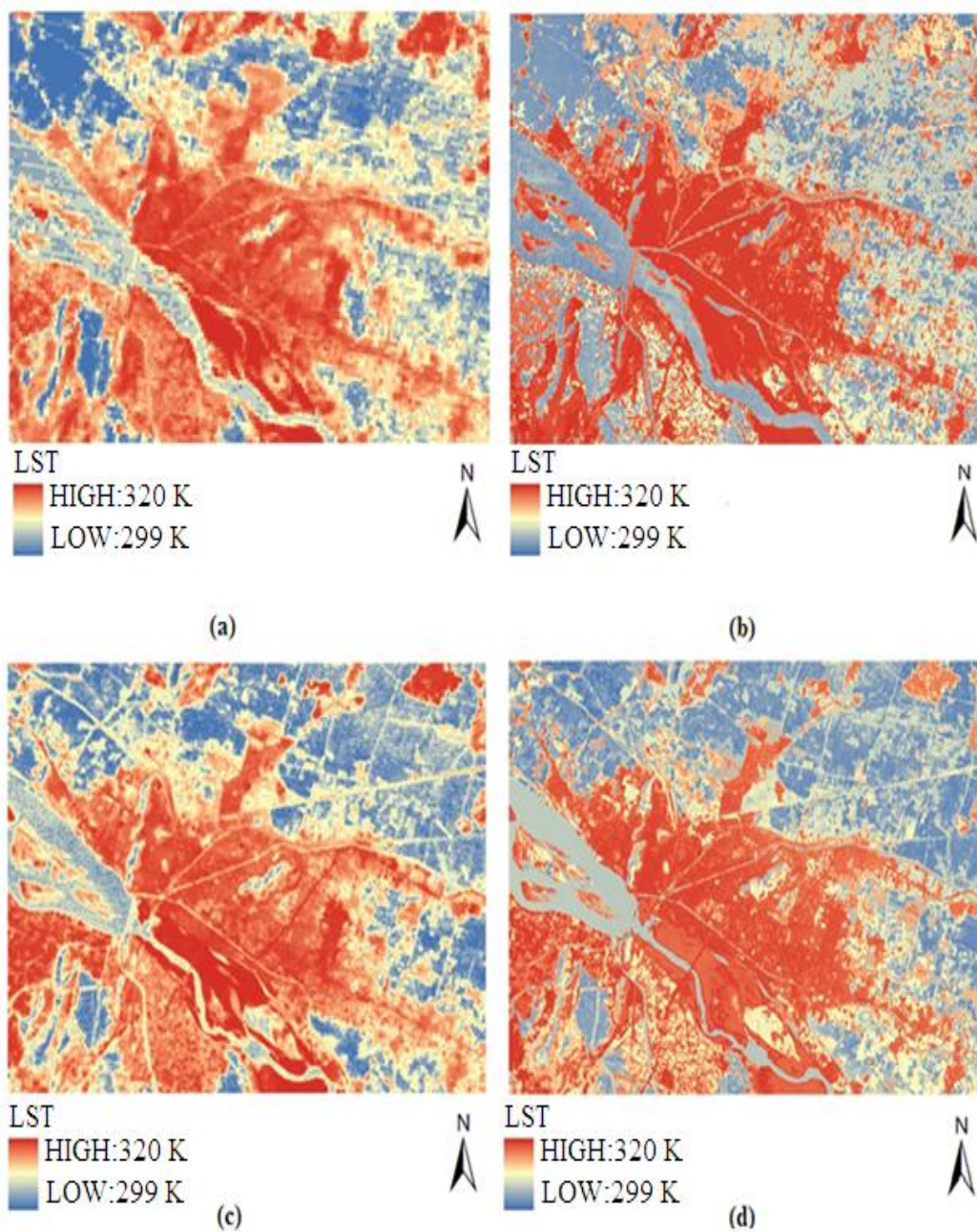


Fig. 7(a) Actual LST image for 2001 (b) Predicted LST image from ANN model for 2001
(c) Actual LST image for 2010 (d) Predicted LST image from ANN model for 2010

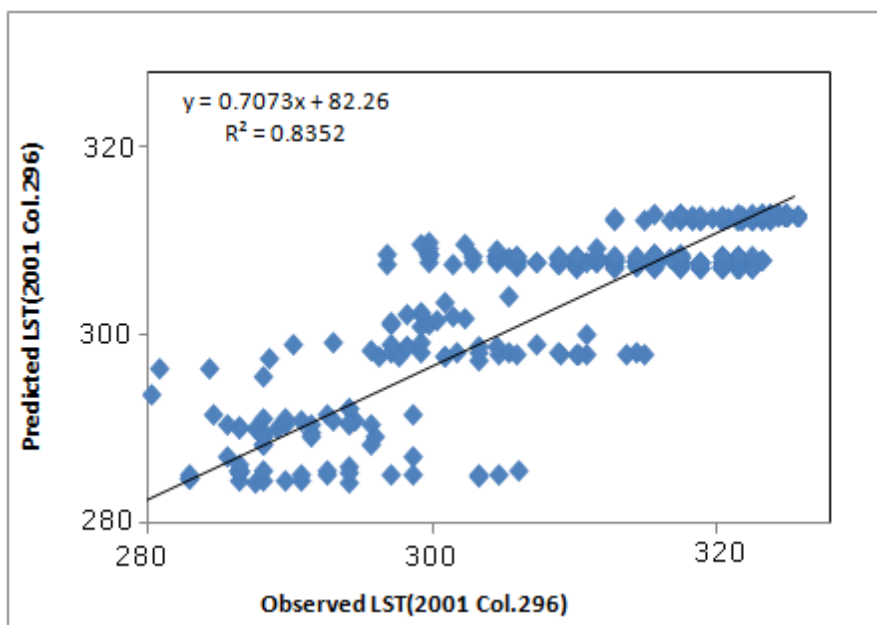


Fig. 8(a) Scatter plot between observed (actual) and predicted values for a randomly selected column in the 2001 image data

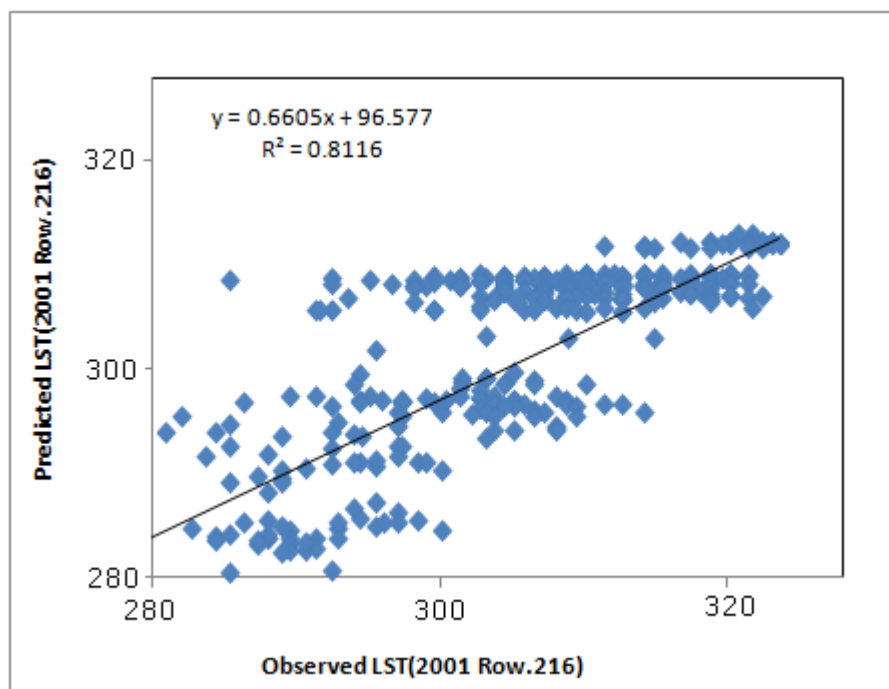


Fig. 8(b) Scatter plot between observed (actual) and predicted values for a randomly selected Row in the 2001 image data

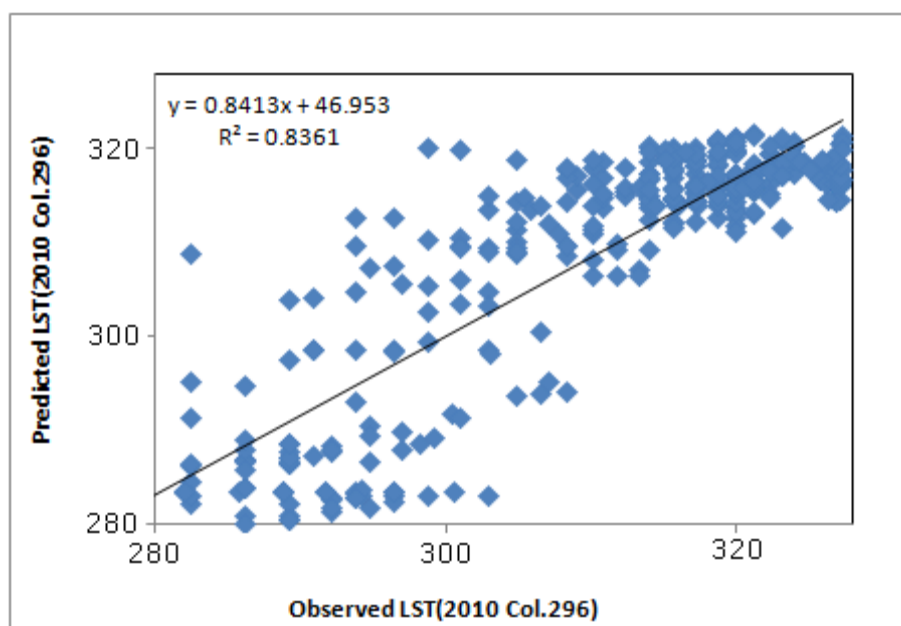


Fig. 8(c) Scatter plot between observed (actual) and predicted values for a randomly selected column in the 2010 image data

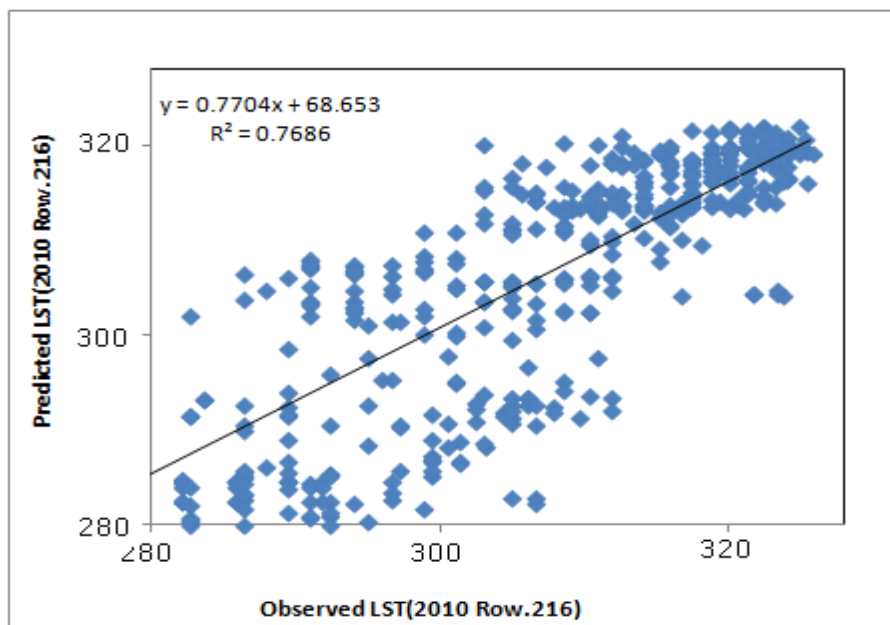


Fig. 8(d) Scatter plot between observed (actual) and predicted values for a randomly selected column in the 2010 image data

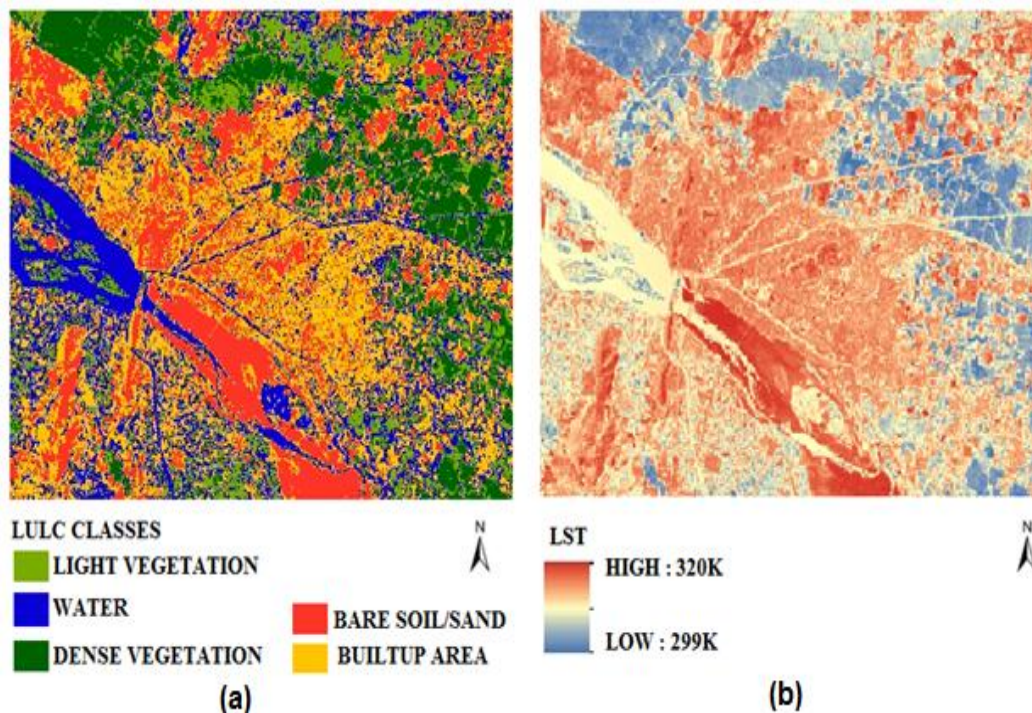


Fig. 9(a) LULC image for 2015 (b) Predicted LST image from ANN model for 2015

5 CONCLUSIONS

Land surface temperature (LST) retrieval is essential for the study and mitigation of urban heat island effect. For obtaining LST, satellite image with thermal band is required and specialized procedures are to be adopted. LST basically depends on the type of land use/cover (LULC). In this research, an artificial neural network (ANN) model is developed to predict LST from merely land use/cover (LULC) image, which does not require thermal band data. For this work Landsat images of the study area are processed to develop LULC image with five classes using supervised classification method. Further normalized difference vegetation index (NDVI) and LST images are developed for the same area. A basic ANN model with LULC image data as input and LST as output has been developed. The entire image data has been converted to digital data for use in the model and the output is again converted back to image. The model efficiency is improved by including, elevation and Latitude and Longitude as additional input layers. Training and testing of the model are carried out using image data of 2001 and 2010 respectively. From regression analysis of the input and output data it is found that the goodness-of-fit statistics are satisfactory and model can predict well. The best model with four input layers is obtained at four

hidden neuron layers and for this the model efficiency is 81.621% and R^2 value between observed and predicted values is 0.821. The model can be used as a good tool to develop LST image from LULC image without thermal band data. The model can also be used to predict the future LST image from the predicted future LULC images which will be beneficial to the urban planners for mitigating the adverse effects of the urban heat island.

Acknowledgement

All the remote sensing satellite data were procured from US Geological Survey (USGS) through Earthexplorer website and by contacting them. The authors wish to acknowledge USGS for their support.

6 REFERENCES

1. Steve Kardinal .J , Wong, N.H., Hagen. E., Anggoro, R., & Hong, Y. (2007). The influence of land use on the urban heat island in Singapore, *Habitat International*, 31, 232-242
2. Fei Yuan & Marvin E. Bauer. (2007), Comparison of impervious surface area and normalized difference vegetation index as indicators of surface urban heat island effects in Landsat imagery, *Remote Sensing of Environment*, 106 , 375-386.
3. Oke, T. R. (1982). The energetic basis of the urban heat island. *Quarterly Journal of the Royal Meteorological Society*, 108, 1-24.
4. Owen, T.W., Carlson, T. N., & Gillies, R. R. (1998): An assessment of satellite remotely-sensed land cover parameters in quantitatively describing the climatic effect of urbanization, *International Journal of Remote Sensing*, 19(9), 1663-1681
5. Voogt, J. A., & Oke, T. R. (2003). Thermal remote sensing of urban areas. *Remote Sensing of Environment*, 86, 370-384.
6. Streutker, D. R. (2002). A remote sensing study of the urban heat island of Houston, Texas. *International Journal of Remote Sensing*, 23, 2595-2608.
7. Livada, I., Santamouris, M., & Assimakopoulos, M. N. (2007). On the variability of summer air temperature during the last 28 years in Athens. *Journal of Geophysical Research*, 112, D12103.
8. Livada, I., Santamouris, M., Niachou, K., Papanikolaou, N., & Mihalakakou, G. (2002). Determination of places in the great Athens area where the heat island effect is observed. *Theoretical and Applied Climatology*, 71(3-4), 219-230.
9. Mihalakakou, M., Santamouris, N., & Papanikolaou, C. (2004). Cartalis simulation of the urban heat island phenomenon in Mediterranean climates. *Pure and Applied Geophysics*, 161, 429-451.

10. Santamouris, M., Paraponiaris, K., & Mihalakakou, G. (2007). Estimating the ecological footprint of the heat island effect over Athens, Greece. *Climate Change*, 80, 265-276.
11. Gobakis, K., Kolokotsa, D., Synnefa, A., Saliari, M., Giannopoulou, K. & Santamouris, M. (2011). Development of a model for urban heat island prediction using neural network Techniques, *Sustainable Cities and Society*, 1, 104-115.
12. Mirzaei, P. A., & Haghghat, F. (2010). Approaches to study urban heat island-Abilities and limitations. *Building and Environment*, 45(10), 2192-2201
13. Wang, W.C., Zeng, Z., & Karl, T. R. (1990). Urban heat islands in China. *Geophysical Research Letters*, 17, 2377-2380.
14. Weng, Q. (2009). Landscape as a continuum: An examination of the urban landscape structures and dynamics of Indianapolis city, 1991–2000. *International Journal of Remote Sensing*, 30(10), 2547-2577
15. Weng, Q. (2001). A remote sensing-GIS evaluation of urban expansion and its impact on surface temperature in the Zhujiang Delta, China. *International Journal of Remote Sensing*, 22(10), 1999-2014.
16. Weng, Q. (2003). Fractal analysis of satellite-detected urban heat island effect. *Photogrammetric Engineering and Remote Sensing* 69 (5), 555-566.
17. Weng, Q., Lu, D., & Schubring, J. (2004). Estimation of land surface temperature–vegetation abundance relationship for urban heat island studies. *Remote Sensing of Environment*, 89, 467–483.
18. Carlson, T.N., Gillies, R.R. & Perry, E.M., 1994. A method to make use of thermal infrared temperature and NDVI measurements to infer surface water content and fractional vegetation cover. *Remote Sensing Reviews*, 9 (1-2), 161-173.
19. Kustas, W.P., Norman, J.M., Anderson, M.C. & French, A.N. (2003). Estimating sub pixel surface temperatures and energy fluxes from the vegetation index-radiometric temperature relationship. *Remote sensing of Environment*, 85 (4), 429-440.
20. Lambin, F.F. & Ehrlich, D. (1996). The surface temperature-vegetation index space for land use and land cover change analysis. *International Journal of Remote Sensing*, 17 (3), 463- 487.
21. Sobrino, J.A., Jimenez Munoz, J.C. & Paolini, L., (2004). Land surface temperature retrieval from LANDSAT TM 5. *Remote Sensing of Environment*, 90 (4), 434-440.
22. Gillies, R. R., & Carlson, T. N. (1995). Thermal remote sensing of surface soil water content with partial vegetation cover for incorporation into climate models. *Journal of Applied Meteorology*, 34, 745-756.
23. Gillies, R.R., Carlson, T.N., Cui, J., Kustas, W.P. & Humes, K.S. (1997). A verification of the 'triangle' method for obtaining surface soil water content and energy fluxes from remote measurements of the Normalized Difference

- Vegetation index (NDVI) and surface radiant temperature. *International Journal of Remote Sensing*, 18 (5), 3145-3166.
24. Goward, S.N., Xue, Y. & Czajkowski, K.P. (2002). Evaluating land surface moisture conditions from the remotely sensed temperature/vegetation index measurements: An exploration with the simplified biosphere model. *Remote Sensing of Environment*, 79 (2-3), 225-242.
 25. Arthur, S.T., Carlson, T. N., & Ripley, D. A. J. (2000). Land use dynamics of Chester County, Pennsylvania, from a satellite remote sensing perspective. *Geocarto International*, 15(1), 25-35.
 26. Carlson, T.N., Arthur, S.T. (2000). The impact of land use - land cover changes due to urbanization on surface microclimate and hydrology: A satellite perspective. *Global and Planetary Change*, 25 (1-2), 49-65.
 27. Civco, D. L., Hurd, J. D., Wilson, E. H., Arnold, C. L., & Prisloe, M. P. Jr. (2002). Quantifying and describing urbanizing landscapes in the northeast United States. *Photogrammetric Engineering and Remote Sensing*, 68(10), 1083-1090.
 28. Yang, L., Huang, C., Homer, C. G., Wylie, B. K., & Coan, M. J. (2003). An approach for mapping large-scale impervious surfaces: Synergistic use of Landsat-7 ETM+ and high spatial resolution imagery. *Canadian Journal of Remote Sensing*, 29, 230-240.
 29. Arnold, C. L., & Gibbons, C. J. (1996). Impervious surface coverage: The emergence of a key environmental indicator. *Journal of the American Planning Association*, 62(2), 243-258.
 30. Carnahan, W. H., & Larson, R. C. (1990). An analysis of an urban heat sink. *Remote Sensing of Environment*, 33, 65-71
 31. Kim, H. H. (1992). Urban heat island. *International Journal of Remote Sensing*, 13, 2319-2336.
 32. Matson, M., Mc Clain, E.P., McGinnis, D.F. & Pritchard, J.A.(1978). Satellite detection of urban heat island. *Mon. Weather Rev.* 106, 1725-1734.
 33. Vukovich, F.M. (1983). An analysis of the ground temperature and reflectivity pattern about St. Louis, Missouri, using HCMM satellite data. *J. Appl. Meteorology*. 22, 560- 571.
 34. Roth, M., Oke, T.R., & Emery, W.J. (1989). Satellite-derived urban heat island from three coastal cities and the utilization of such data in urban climatology. *International Journal of Remote Sensing*, 10, 1699-1720.
 35. Jianga. D., Zhanga Y., Hua. X., Zenga. Y., Tanb. J. & Shao. D. (2004). Progress in developing an ANN model for air pollution index forecast. *Atmospheric Environment*, 38, 7055-7064.
 36. Grivas. G ., & Chaloulakou. A. (2006). Artificial neural network models for prediction of PM10 hourly concentrations, in the Greater Area of Athens, Greece. *Atmospheric Environment*, 40, 1216-1229.
 37. Cybenko, G. (1989). Approximation by superposition of a sigmoidal function. *Math Control Signal Syst.*, 2, 303-14

38. Diaz, G., Sen, M., Yang, K. T., McClain, R. L. (2001). On-line training of artificial neural Networks for control of a heat exchanger test facility, *Proc. National Heat Transfer Conf.*, 1, 1671-1679.
39. Topalli, K. A. & Erkmén, I. (2003). A hybrid learning for neural networks applied to short term load forecasting. *Neurocomputing*, 51, 495-500.
40. Islamoglu, Y. A. (2003). New approach for the prediction of the heat transfer rate of the wire on-tube type heat exchanger – use of an artificial neural network model. *Appl. Therm. Eng.*, 23, 243-249.
41. Gwo-Ching, Liao & Ta-Peng, Tsao. (2004). Application of fuzzy neural networks and artificial intelligence for load forecasting. *Electric Power System Research*, 70, 237-244.
42. Yalcinoz, T., Eminoglu, U. (2005). Short term and medium term power distribution load forecasting by neural networks. *Energy Conversion and Management*, 46, 1393-1405.
43. Lauret, Philippe., Eric, Fock., Rija, Randrianarivony., Jean-François & Manicom, R. (2008). Bayesian neural network approach to short time load forecasting. *Energy Conversion Management*, 49, 1156-1166.
44. Jassar, S., Liao, Z., & Zhao, L. (2009). Adaptive neuro-fuzzy based inferential sensor model for estimating the average air temperature in space heating systems. *Building and Environment*, 44, 1609-1616.
45. Gardner, M. W., & Dorling, S. R. (1998). Artificial neural networks (the multilayer perceptron) - A review of applications in the atmospheric sciences. *Atmospheric Environment*, 32, 2627–2636.
46. Dash, P., Gottsche, F.M., Olesen, F.S. & Fischer, H. (2002). Land surface temperature and emissivity estimation from passive sensor data: Theory and practice, current trends. *International Journal of Remote Sensing*, 23 (13), 2563-2594.
47. Landsat Project Science Office. (2002). Landsat 7 science data user's handbook. *Goddard Space Flight Center*, Available from: www address: http://ltpwww.gsfc.nasa.gov/IAS/handbook/handbook_oc.html.
48. Gillespie, A., Rokugawa, S., Matsunaga, T., Cothorn, J. S., Hook, S., & Kahle, A.B. (1998). A temperature and emissivity separation algorithm for advanced space borne thermal emission and reflection radiometer (ASTER) images. *IEEE Transactions on Geoscience and Remote Sensing*, 36, 1113-1126.
49. Becker, F., & Li, Z. (1995). Surface temperature and emissivity at various scales: Definition, measurement and related problems. *Remote Sensing Reviews*, 12, 225-253.
50. Watson, K. (1992). Spectral ratio method for measuring emissivity. *Remote Sensing of Environment*, 42 (2), 113-116.
51. Kealy, P.S. & Gabell, A.R. (1990). Estimation of emissivity and temperature using alpha coefficients. In: *Proceedings of Second TIMS Workshop. JPL Pub. 90-95, Jet Propulsion Laboratory, Pasadena, California*, 11-15.

52. Valor, E. & Cassells, V. (1996). Mapping land surface emissivity from NDVI: Application to European, African, and South American areas. *Remote Sensing of Environment*, 57 (3), 167-184.
53. Snyder, W.C., Wan, Z., Zhang, Y., & Feng, Y.Z.(1998). Classification-based emissivity for land surface temperature measurement from space. *International Journal of Remote Sensing* 19 (14), 2753-2774.
54. Liang, S. (2001). An optimization algorithm for separating land surface temperature and emissivity from multispectral thermal infrared imagery. *IEEE Transactions on Geoscience and Remote Sensing*, 39 (2), 264-274.